Exploring the magnetic phase diagram of dysprosium with neutron diffraction

J. Yu,[1,*] P. R. LeClair,[1] G. J. Mankey,[1] J. L. Robertson,[2] M. L. Crow,[2] and W. Tian[3]

[1]*Center for Materials for Information Technology, The University of Alabama, Tuscaloosa, Alabama 35487, USA*

[2]*Instrument and Source Division, Oak Ridge National Laboratory, Oak Ridge, Tennessee 37831, USA*

[3]*Quantum Condensed Matter Division, Oak Ridge National Laboratory, Oak Ridge, Tennessee 37831, USA*

With one of the highest intrinsic magnetic moments ($10.6\,\mu_B$/atom) among the heavy rare-earth elements, dysprosium exhibits a rich magnetic phase diagram, including several modulated magnetic phases. Aided by the Ruderman-Kittel-Kasuya-Yosida interaction, the magnetic modulations propagate coherently over a long range. Neutron diffraction experiments were performed to determine the microscopic magnetic origin of the field induced phases in bulk Dy as a function of temperature, covering regions of the well-known ferromagnetic, helical antiferromagnetic, fan phases, and several possible new phases suggested by previous studies. A short-range ordered fan phase was identified as the intermediate state between ferromagnetism and long-range ordered fan. In a field of 1 T applied along the *a* axis, the temperature range of a coexisting helix/fan phase was determined. The magnetic phase diagram of Dy was thus refined to include the detailed magnetic origin and the associated phase boundaries. Based on the period of the magnetic modulation and the average magnetization, the evolution of the spin arrangement upon heating was derived quantitatively for the modulated magnetic phases.

PACS number(s): 75.25.−j, 71.20.Eh, 75.30.Kz

I. INTRODUCTION

The magnetic rare-earth materials present opportunities for studying fundamental magnetism and have been extensively investigated for decades. They undergo complex phase transitions between a range of diverse magnetic phases through various temperatures and magnetic fields. Heavy rare-earth elements with more than half-filled $4f$ shells exhibit several intermediate phases during the transitions from the high-temperature paramagnetic (PM) phases to the low-temperature ferromagnetic (FM) phases, excluding Gd, which orders ferromagnetically near room temperature [1]. The most interesting but unique feature for the intermediate magnetic phases is the so-called modulated magnetic structure, which involves an oscillatory arrangement of spins from layer to layer [1]. The modulated magnetic structure in heavy rare earth can have an oscillatory moment either in amplitude or orientation or both. The helical configuration in Dy is an example of the oscillatory orientation [2], while the conical configuration in Er is the case of both oscillatory orientation and amplitude [3]. It is well known that the interaction between the localized $4f$ electrons through conduction electrons contributed by the $5d$ and $6s$ shells, known as the indirect Ruderman-Kittel-Kasuya-Yosida (RKKY) interaction, is primarily responsible for such oscillatory arrangements [4–6]. However, the exact magnetic structure in rare-earth materials can be the effect of the RKKY interaction perturbed by the anisotropic crystal field and magnetoelastic interactions [7,8]. Moreover, the competition between the interactions is temperature and field dependent, resulting in the complex magnetic phase diagram.

The identification of these modulated magnetic structures in heavy rare-earth materials was pioneered by Koehler *et al.* in the 1960s via neutron diffraction and delivered a general understanding on the basic mechanism [2,9–11]. By the 1990s, the magnetic structures in Ho have been largely revealed. A

stable helifan phase was predicted by self-consistent mean-field calculations [12] and later verified by neutron diffraction experiments [13] as an intermediate phase between the helix and fan phases when a certain range of magnetic field is applied in the basal plane. A spin-slip model was developed and successfully explained the harmonics around the magnetic satellites observed in both x-ray magnetic scattering [14] and neutron diffraction [15] and also agreed well with the theoretical calculations [16]. However, the understanding of the magnetic phase diagram of Dy, the neighbor of Ho in the periodic table, was not so successful.

In zero magnetic field, bulk Dy is PM at room temperature, and the atomic spins order in an incommensurate helix below the Néel temperature of 179 K. At the Curie temperature of around 86 K, the helical magnetic state goes through a first-order phase transition and collapses to the FM state [2]. The period of the magnetic modulation in bulk Dy is temperature dependent within the helical magnetic region (86–179 K). In terms of the turn angle, it decreases monotonically from 44° to 27° before it collapses into the FM state where the turn angle is essentially 0°.

In a nonzero magnetic field, however, a couple of candidates of the intermediate phases have been reported between the PM, helical magnetic, and FM states. With a field applied along the *a* axis, the appearance of a fan phase was confirmed by isothermal magnetization curves [17] and neutron diffraction [18]. An extra phase boundary was detected in the middle of the fan phase via resistivity measurements, but the nature of the related phases was unclear [19]. Chernyshov *et al.* [20] observed many anomalies during a careful investigation on the magnetocaloric effect, magnetization, ac susceptibility, and heat capacity of single-crystal Dy, and mapped out the most detailed version of the magnetic phase diagram for Dy, which included a spin-flop phase, a vortex phase, and a few possible new phases. However, the neutron diffraction measurements on Dy in the past have covered a few discrete regions in the phase diagram only to identify the presence of the helix, fan, and FM phases [2,18]. Further experiments are necessary in

---

*Corresponding author: jyu@mint.ua.edu

TABLE I. The list of the measurement conditions of the neutron diffraction experiments performed on the ^{163}Dy crystal. The field is applied along the a axis of Dy crystal. PM: paramagnetic state; FM: ferromagnetic state.

Applied field	Temperature ranges	Heating/cooling	Covered phases
0	5–260 K	Heating and cooling	FM, helix, PM
1.0 T	119–177 K	Heating	FM, helix, fan, PM
1.5 T	115–190 K	Heating	FM, fan, PM

order to confirm the existence of the new phases and explore the magnetic nature of them.

The magnetic phase transitions in bulk Dy are accompanied by a series of structural transitions. The structural transition and the magnetic transition can be coupled or decoupled at different temperatures. The lattice parameter of Dy along the c axis decreases between the Curie temperature (86 K) and the Néel temperature (179 K), exhibits a minimum at the Néel temperature, and increases with temperature above the Néel temperature [21]. Upon heating in zero field, an orthorhombic-hexagonal close-packed (hcp) transition occurs at the Curie temperature, along with a discontinuity in the c axis lattice parameter [21]. When a moderate magnetic field is applied in the basal plane of Dy crystal, the c axis discontinuity shifts to a higher temperature, together with the FM-helix transition, suggested by the magnetization measurements [17]. However, the orthorhombic-hcp transition appears independent of the field and always occurs at the Curie point [20].

More detailed studies of the magnetic modulations became feasible in recent years with advances in neutron scattering techniques in terms of the increased neutron flux and the flexibility of the instruments [22]. Here, we discuss neutron diffraction results measured along the c axis of a Dy crystal throughout the temperatures covering the FM phase to the PM phase at different applied fields, aiming to investigate the detailed magnetic phase diagram of bulk Dy, as well as the nature of the possible new phases.

II. EXPERIMENTAL

A single-crystal ^{163}Dy with a mass of ~30 g was used for the neutron diffraction experiment. This isotope was selected because it has the lowest neutron absorption among the most abundant isotopes of Dy [23]. The measurements were performed at the Fixed-Incident-Energy (14.6 meV) Triple-Axis Spectrometer (HB-1A) located at the High Flux Isotope Reactor (HFIR), Oak Ridge National Laboratory (ORNL). The PG (002) analyzer used gives a typical energy resolution of ~1 meV. Since the magnetic easy plane is the basal plane for the hexagonal Dy lattice, the complex magnetic structures tend to oscillate along the c axis due to the competition of the interactions between the neighboring basal planes. Therefore, the scans were carried out such that the scattering vectors were parallel to the c axis of the Dy crystal in order to probe the magnetic modulations propagating along the c axis. The measurements were performed as a function of temperature with three different fields (0, 1, and 1.5 T) applied along the a axis of the crystal, covering the PM, FM, helical, fan phases, and the possible intermediate phases in between, based on

the phase diagram in Ref. [20]. Table I lists the measurement conditions of the neutron diffraction experiment.

III. RESULTS AND DISCUSSION

A. Overview of the results

The raw data of the neutron diffraction scans at a fixed field can be plotted on a single three-dimensional intensity map. Figure 1 shows the results of the scans at the field of 1 T. The horizontal axis is the scattering vector Q around the Dy (0002) [24] nuclear diffraction peak. The vertical axis is the temperature of the scan. During the scan, the neutrons can be diffracted by both the nuclei and the magnetic moments of Dy, and also by the sample holder. Therefore, the intensities in Fig. 1 include the contributions from the nuclear, magnetic, and background signals.

Each of the intensity ridges in Fig. 1 represents the evolution of a diffraction peak as a function of temperature. Figure 2 shows an example of the diffraction pattern of a single Q scan at a given temperature (170 K) and field (1 T). The Q position of a peak is equal to the magnitude of the reciprocal vector of the modulation giving rise to the peak. The temperature independent peak at $Q \approx 2.7\,\text{Å}^{-1}$ (Fig. 1) is identified to
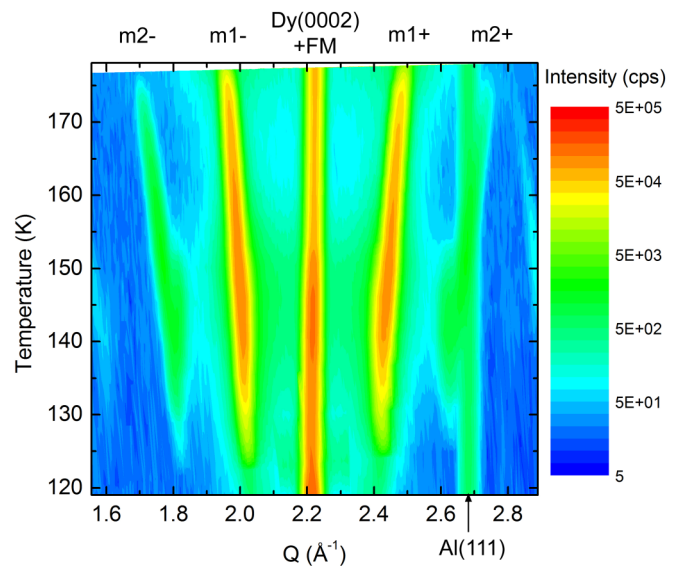

FIG. 1. (Color online) The raw neutron diffraction patterns of scans along the c axis of the ^{163}Dy crystal at various temperatures with the field of 1 T applied along the a axis. The Dy (0002) nuclear peak, the FM diffraction peak, the first-order magnetic satellites ($m1\pm$), the second-order satellites ($m2\pm$), and the Al (111) nuclear peaks are marked in the plot.
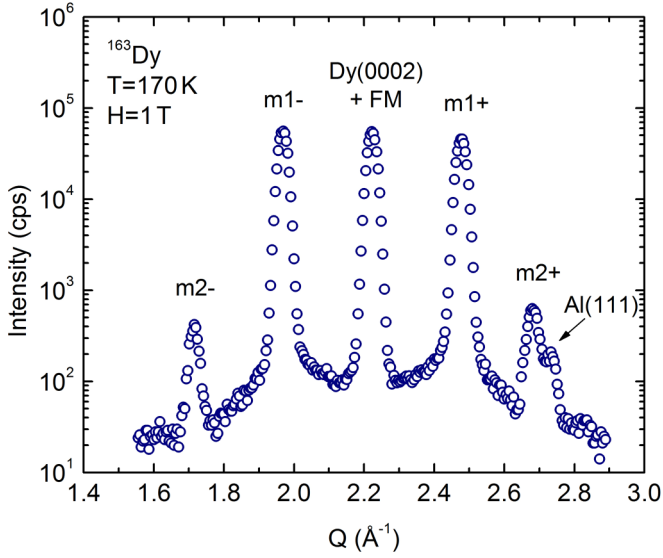
FIG. 2. (Color online) The raw neutron diffraction pattern of a single Q scan along the c axis of the ^{163}Dy crystal at a fixed temperature (170 K) with the field of 1 T applied along the a axis.

FIG. 3. (Color online) The neutron diffraction pattern of pure nuclear origin measured at 275 K with no field applied.

originate from the Al sample holder, since it matches the lattice spacing of the Al (111) planes. The central diffraction peak at $Q \approx 2.2\,\text{Å}^{-1}$ is associated with the modulation whose period equals the lattice spacing along the c axis of the Dy crystal. This periodicity could stem from two possible scattering planes: (a) the Dy nuclei in the (0002) atomic planes, and (b) the magnetic moments of Dy in the (0002) atomic planes when they are all ferromagnetically aligned. The diffraction peak due to the former is temperature independent whereas the intensity from the latter is proportional to the square of the net magnetization of the sample. The position of the central diffraction peak varies slightly with temperature, reflecting the temperature dependence of the lattice parameter along the c axis of the Dy crystal. The central peak in Fig. 1 shifts to a higher Q as temperature increases. The other peaks, bracketing evenly and symmetrically about the central peak, are the satellites of pure magnetic origin. A pair of first-order magnetic satellites (marked as $m1+$ and $m1-$) and two second-order satellites ($m2+$ and $m2-$) can be seen in Fig. 2. The positions of the magnetic satellite peaks are temperature dependent for Dy and can be related to the average period (Λ_m) of the magnetic modulation in the crystal by

$$\Delta Q = \frac{2\pi n}{\Lambda_m}, \tag{1}$$

where n is the order of the magnetic satellite and ΔQ is the separation between the nuclear diffraction peak and the nth-order magnetic satellite.

The diffraction peaks observed for the PM state of Dy are of pure nuclear origin. In Fig. 3, at the temperature of 275 K, well above the Néel temperature (179 K) of Dy, only the Dy (0002) and Al (111) nuclear peaks show up. The nuclear diffraction peaks are nearly perfect Gaussians with insignificant diffuse scattering. The nuclear diffraction peaks provide information about the modulation of the chemical periodicity, i.e., the interplanar spacing, along the c axis of the hexagonal crystal,
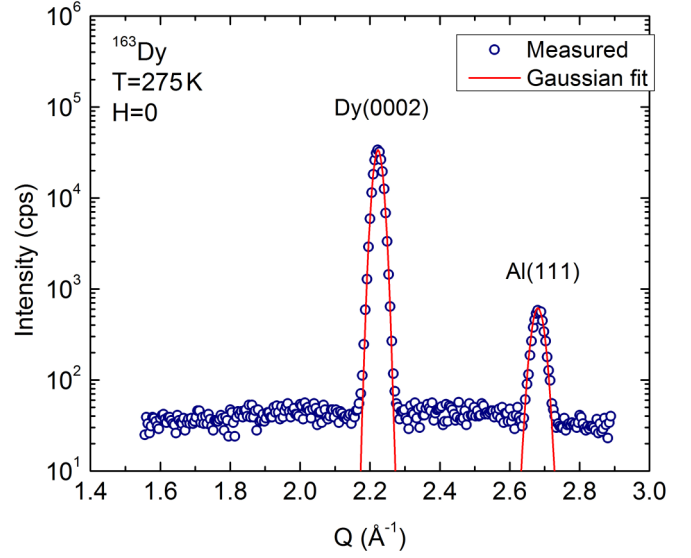
corresponding to the position of the Dy (0002) peak. The temperature dependence of the interplanar spacing is discussed in Sec. III B.

Since the integrated intensity of the nuclear diffraction peak is temperature independent, it is reasonable to subtract the diffraction pattern in Fig. 3 from any diffraction patterns of lower temperatures to obtain the pure magnetic signal. However, the subtraction cannot be done directly because the central diffraction peaks are not perfectly aligned at the same Q position, owing to the temperature dependence of the lattice spacing between the Dy (0002) planes. The position of the central diffraction peak $Q_0(T)$ can be written as a function of temperature

$$Q_0(T) = \frac{2\pi}{c(T)/2}, \tag{2}$$

where $c(T)$ is the lattice parameter along the c axis. This issue can be solved by converting the horizontal axis to the reduced wave vector $[000L]$, where L is the ratio between the scattering vector and the reciprocal vector of the c axis, i.e.,

$$L = \frac{Q \cdot c}{2\pi}. \tag{3}$$

Therefore, the position of the central diffraction peak in terms of the reduced wave vector becomes temperature independent, i.e.,

$$L_0 = \frac{Q_0 \cdot c}{2\pi} = 2. \tag{4}$$

A constant background intensity was also subtracted from the raw signal in order to retrieve the clean magnetic signal.

During the heating and cooling process, the expansion or contraction of the sample holder may misalign the c axis of the crystal from the scattering vector, giving lower intensities of the diffraction peaks. Therefore, the crystal was realigned at each temperature before the scan. However, for some of the temperature points, the crystal showed further movement after
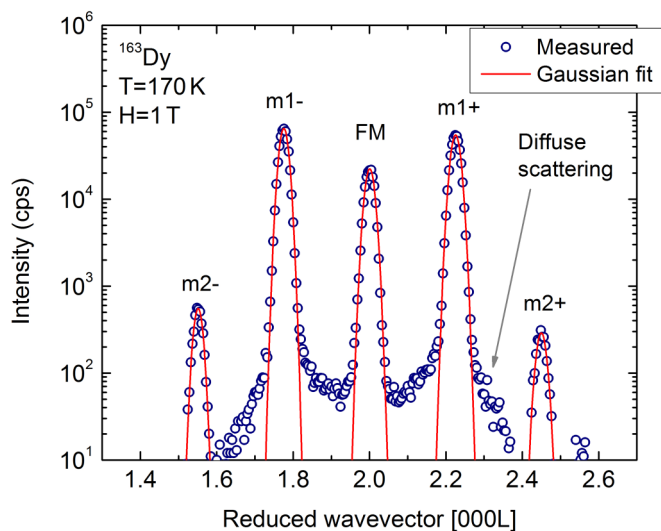
FIG. 4. (Color online) The neutron diffraction pattern of pure magnetic origin obtained by subtracting the nuclear contributions (Fig. 3) from the raw data (Fig. 2). The horizontal axis has been converted to the reduced wave vector [000L], in order to align the FM peaks.

FIG. 5. (Color online) The temperature dependence of the interplanar spacing along the c axis of the Dy crystal in different fields (0, 1, and 1.5 T) applied along the a axis. The dash lines indicate the Curie temperature (89 K) and the Néel temperature (179 K).

the realignment. The intensity of the diffraction peaks for these temperature points were corrected manually.

After the subtraction of the nuclear signal, the pattern of the pure magnetic diffraction is plotted in Fig. 4. The central diffraction peak at $L = 2.0$ stems from the FM component in the crystal, while the magnetic satellites are the result of the magnetic modulations along the c axis. The magnetic peaks could be accurately fitted by Gaussian functions. The width of the Gaussian function is approximately the same for all diffraction peaks, as it is defined by the instrument resolution ($\Delta L \approx 0.02 - 0.03$). In addition, noticeable diffuse scattering was observed around the FM diffraction peak and the first-order satellite peaks, indicating the inhomogeneity in the magnetic structures. The detailed discussions of magnetic diffraction patterns at various temperatures and fields are given in Secs. III C through III E.

B. Temperature dependence of the lattice parameters of ^{163}Dy in various applied fields

The interplanar spacing along the c axis of the Dy crystal is plotted as a function of temperature in Fig. 5 for different applied fields (0, 1, and 1.5 T). When no field was applied, the lattice spacing was measured for both heating and cooling, and no significant thermal hysteresis was observed. The curve is separated into three stages by two critical temperatures, the Curie temperature (89 K) and the Néel temperature (179 K). Above 179 K, the c axis of the Dy crystal expands as the temperature increases. In contrast, the c axis contracts as the temperature increases from 89 to 179 K. At 89 K, where the first-order helix-FM transition occurs, there is an abrupt expansion of the c axis. The same behavior has been measured by Darnell [21] and suggested by Evenson and Liu [8] as the primary contribution, in terms of the magnetostrictive interactions, for the helix-FM phase transition and the temperature dependence of the pitch of the helix.
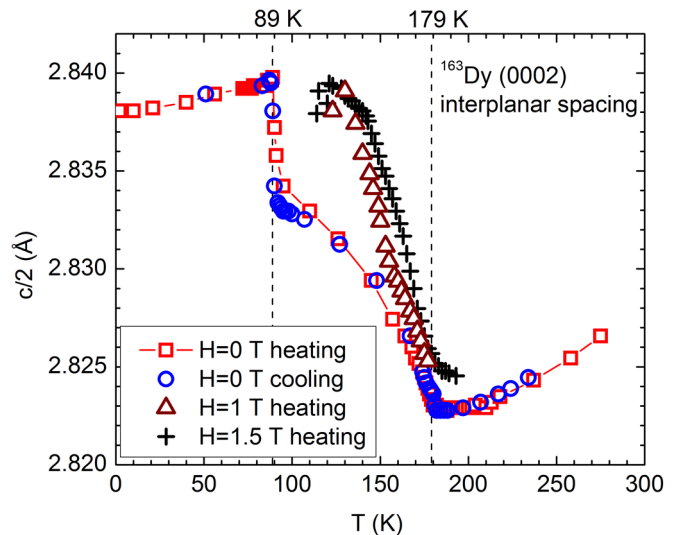
The lattice parameters in a nonzero field (1 and 1.5 T) were only measured between 110 and 190 K. The field applied along the a axis induces a further expansion of the c axis from the zero-field values, as shown in Fig. 5. The field dependence of the c axis spacing is in good agreement with the magnetostriction study by Rhyne [25] and Rhyne and McGuire [26]. At around 130 K, the c axis spacing has reached 2.838 Å, the value associated with FM in zero field. Given that a higher helix-FM transition temperature has been reported with nonzero field applied [2,20], it is evident that the c axis (structural) transition is coupled with the helix-FM (magnetic) transition.

C. Magnetic phases and the phase transitions of ^{163}Dy in zero field

The magnetic scattering patterns in zero field covered the FM diffraction peak and a pair of first-order magnetic satellites ($m1-$ and $m1+$). The results were analyzed in terms of the temperature dependence of the integrated intensity [Fig. 6(a)] and the position [Fig. 6(b)] of the diffraction peaks. There was no significant thermal hysteresis for the heating and cooling processes, so the data is shown for heating only. The integrated intensity of the FM peak indicates the amount of ferromagnetically aligned moments in the crystal, whereas the intensities of the magnetic satellites reflect the ordering of the magnetic modulation. The high intensity of the FM peak with the absence of the magnetic satellites confirms the FM phase for temperatures below 89 K. Above 89 K, the FM peak immediately drops to a very low value, while large magnetic satellites arise, suggesting a dominating magnetic modulation with net magnetization close to zero. This magnetic modulation is known as the helical antiferromagnetic structure, which is the ground state of the magnetic hcp lattice if only the RKKY interaction is considered [27]. From 89 to 179 K, the intensity of the magnetic satellites decreases following the Brillouin-type
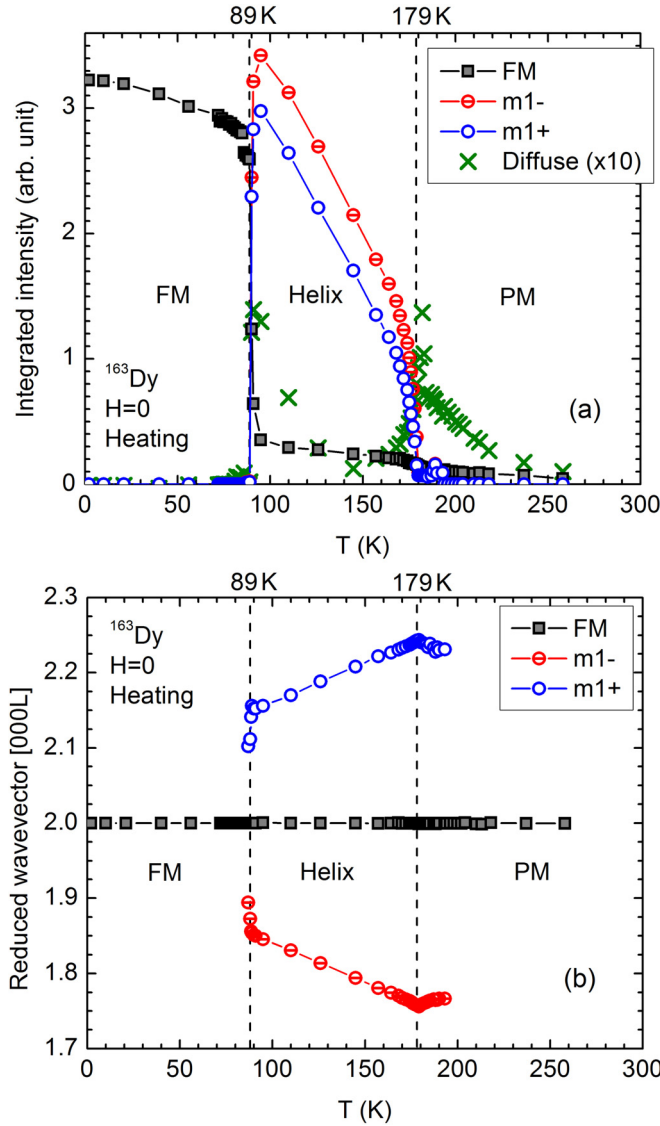
FIG. 6. (Color online) The temperature dependence of (a) the integrated intensity of the magnetic diffraction peaks and the diffuse scattering, and (b) the position of the peaks with no field applied. The intensities of the diffuse scattering have been magnified by 10 times in order to show on the same scale as the FM diffraction peak and the first-order satellites ($m1\pm$). The dash lines indicate the phase boundaries between the FM, helix, and PM phases.
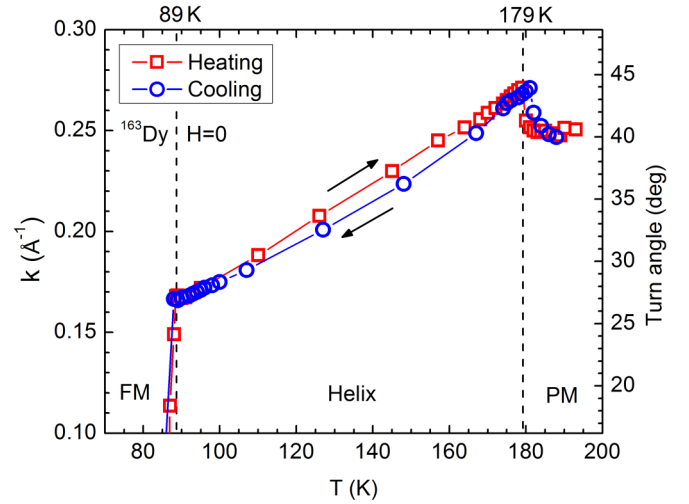

FIG. 7. (Color online) The temperature dependence of the propagation wave vector and the average turn angle of the helix modulation in zero field.

The propagation vector **k**, and the average turn angle of the helix φ, are given by

$$\mathbf{k} = \frac{2\pi}{\Lambda_m}\hat{\boldsymbol{c}},\tag{5}$$

$$\varphi = \frac{c \cdot 180°}{\Lambda_m}.\tag{6}$$

Figure 7 shows the temperature dependence of the propagation wave vector and the average turn angle of the helix for both heating and cooling. The turn angle decreases nearly linearly as the decrease of the temperature. At a given temperature between 110 and 170 K, the turn angles during heating are around 1° larger than those in cooling. As other measurements [2,17,20] on the magnetic phases of the bulk Dy under zero magnetic field suggested, no intermediate phase was detected here.

D. Magnetic phases and the phase transitions of ^{163}Dy in the field of 1 T

The magnetic field applied in the basal plane of the hexagonal Dy crystal is known to not only change the transition temperature between the helical and the FM phases, but also induce intermediate phases [1]. An intermediate fan phase was predicted to emerge naturally between the helical phase and the FM phase in theoretical investigations [28,29] and was later confirmed with experiments [17–19]. However, more intermediate phases are possible based on the phase boundaries constructed in Ref. [20]. The nature of the field induced magnetic phases and the transitions as a function of temperature are investigated here.

With the field of 1 T applied along the *a* axis of the Dy crystal, neutron diffraction scans were performed along the *c* axis at various temperatures from 119 to 177 K. According to the phase diagram in Ref. [20], the FM phase, a possible new phase, the fan phase, the helical antiferromagnetic phase, and a possible vortex phase were covered. Similar to the zero-field case, the temperature dependence of (a) the integrated intensity

temperature dependence. Above 179 K, only small but broad FM peak and magnetic satellites are observed, indicating a dominating PM state with minor helical and FM arrangement with short-range ordering (SRO). The first-order FM-helix transition at 89 K and the second-order helix-PM transition at 179 K are evident from Fig. 6. Moreover, the integrated intensity of the diffuse scattering shows a peak at 89 and 179 K, respectively, further confirming the two phase boundaries. The peak positions shown in Fig. 6(b) provide information about the period of the magnetic modulation in the crystal. The FM peak is coincident with the (0002) nuclear peak since it has the same modulation as the Dy (0002) atomic planes. The period of the helical modulation can be calculated by Eq. (1).
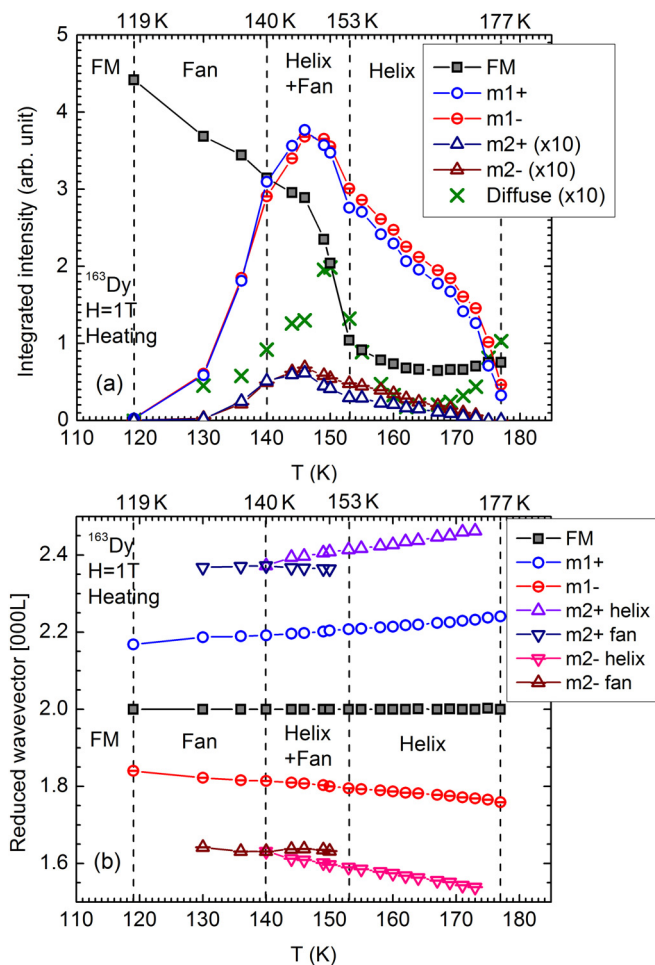
FIG. 8. (Color online) The temperature dependence of (a) the integrated intensity of the magnetic diffraction peaks and the diffuse scattering, and (b) the position of the peaks with 1 T field applied along the a axis of the Dy crystal. The intensities of the second-order magnetic satellites ($m2\pm$) and the diffuse scattering have been magnified by 10 times in order to show on the same scale as the FM diffraction peak and the first-order satellites ($m1\pm$). The dash lines indicate the phase boundaries between the FM, fan, coexisting helix and fan, helix, and PM phases.

and (b) the position of the magnetic diffraction peaks are plotted in Fig. 8. Below 119 K, only the FM phase is present since only a large FM diffraction peak was observed. Between 119 and 145 K, the intensity of the FM peak decreases while the intensities of the magnetic satellites increase. In other words, the net magnetization of the crystal is reduced as the modulated magnetic ordering accumulates. The presence of both an intense FM peak and satellite peaks is a characteristic of the fan phase. The magnetic satellites grow slower upon heating from 119 to 130 K, but faster from 130 to 145 K [Fig. 8(a)]. The fan phase below 130 K appears to be only SRO, while it becomes long-range ordered (LRO) above 130 K. The onset (~130 K) of the LRO fan phase is consistent with the structural transition of the c axis [see Fig. 5]. Between 153 and 177 K, the FM peak drops to a very low value while the magnetic satellites remain relatively intense, suggesting a dominating helical antiferromagnetic state. In our scan

geometry, the magnetization parallel to the c axis does not contribute to the magnetic scattering. Therefore, we are not able to distinguish the helix phase from the vortex phase where the magnetic moments tip out of the basal plane.

Between 140 and 153 K, the second-order magnetic satellite peaks split into a double-peak and the first-order magnetic satellites also appear broader [see Fig. 1 and Fig. 8(b)]. The separation between the double peaks of the second order ranges from 0.026 to 0.032 in terms of the reduced wave vector, which is barely above the resolution limit ($\Delta L \approx 0.02 - 0.03$) of the instrument at the scan region. Therefore, the resolution is not sufficient to distinguish the double peaks of the first order, which would be much closer. The split of the magnetic satellites suggests the coexistence of two magnetic modulations of different wave vectors. This behavior was initially discovered by neutron diffraction at 149 K with the applied field between 0.9 and 1.2 T along the a axis of the Dy crystal [18]. Wakabayashi et al. [18] investigated the origin of the two modulations and concluded that the magnetic satellites closer to the central peak are due to the fan phase and the others are associated with the helix phase. Therefore, we found the helix and the fan phase coexist between 140 and 153 K in the field of 1 T. A closer look of the double peak at the second-order satellite ($m2-$) is shown in Fig. 9. The peak at smaller L arises from the helix while the one at larger L stems from the fan structure. Both peaks can be fitted accurately by a Voigt function with the width consistent with the instrument resolution. The peak positions of the double peak in Fig. 8(b) are determined by the fitting. The peak intensity showed in Fig. 8(a) is the total intensity of both peaks. Two tendencies are observed for the double $m2-$ peaks in Fig. 9 as temperature increases. First, the helix peak grows, and the fan peak decays monotonically upon heating. This illustrates that the phase transition from the fan phase below 140 K to the helix phase above 153 K is of the first order, but is broadened by the inhomogeneity in the crystal. Second, while both of the peaks shift closer to the central peak upon heating, the helix peak is shifting at a higher rate than the fan peak does. The propagation wave vectors (k) for both of the helix and the fan modulations are calculated based on their peak positions and plotted in Fig. 10. Instead of the turn angles, the average period (Λ_m) of the magnetic modulation corresponding to the propagation wave vector is shown as the vertical axis on the right-hand side of Fig. 10 because the average turn angle of the fan modulation cannot be determined without knowing the opening angle.

In the field of 1 T, the fan phase exists between 130 and 153 K, and the average period of the fan modulation stays at around 11 monolayers of the Dy (0002) plane (see Fig. 10). On the other hand, the helix phase appears from about 140 through 177 K, and its average period decreases from 11 to 9 monolayers upon heating. The average turn angles of the helix modulation can be calculated by Eq. (1). However, the fan modulation cannot be described by the turn angle alone. It is necessary to introduce the opening angle for the fan structure. The average turn angle (φ) and the opening angle (Φ) are related by

$$2\Phi = \Lambda_m \varphi. \qquad (7)$$

Here, Λ_m is the average period of the fan modulation in terms of the number of monolayers.
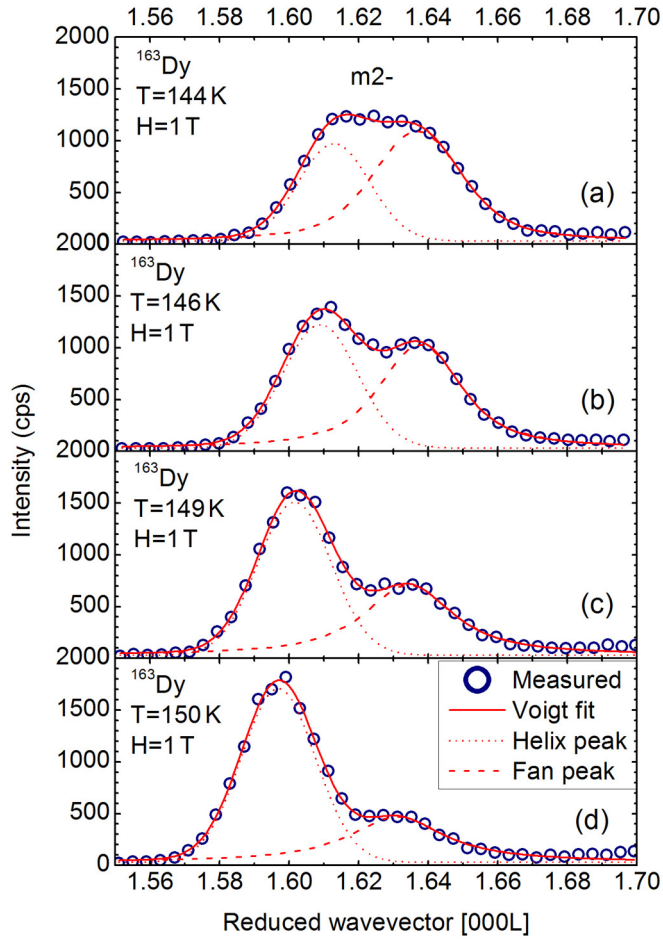
FIG. 9. (Color online) The temperature dependence of the double peaks at the $m2-$ magnetic satellite in a field of 1 T applied along the a axis of the crystal. The peak at the lower L is due to the helix structure, and the one at higher L stems from the fan modulation.
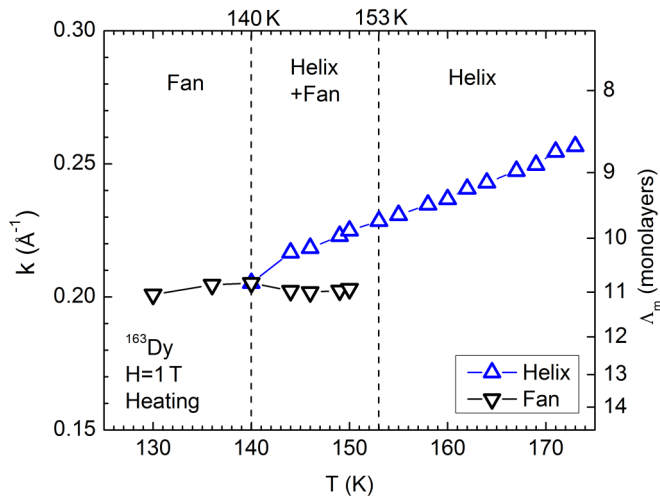

FIG. 10. (Color online) The temperature dependence of the propagation wave vector and the average period of the helix and fan modulations in 1 T field applied along the a axis of the Dy crystal.
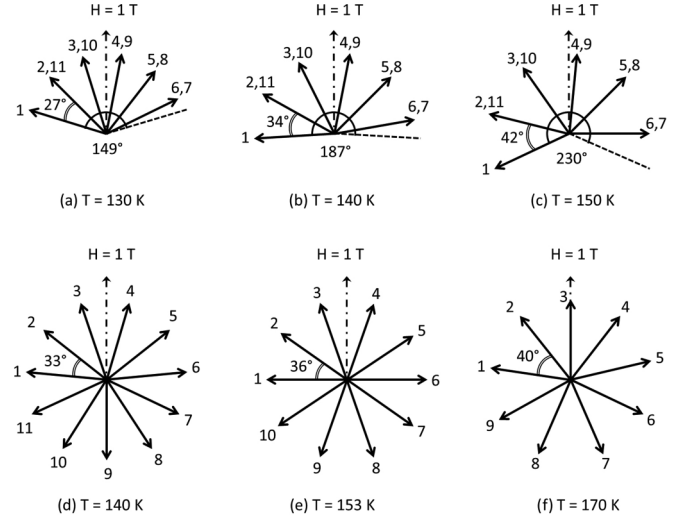

FIG. 11. The evolution of the spin arrangement for (a)–(c) the fan modulation and (d)–(f) the helix modulation upon heating in the field of 1 T. Only one period of the magnetic modulation is shown. The average turn angle and opening angle are estimated based on the magnetization in Ref. [20]. The numbers at the end of the arrows indicate the indices of the Dy (0002) atomic layers.

The average turn angle and the opening angle of the fan modulation were estimated based on the net magnetization of the structure measured at 1 T from Ref. [20]. Assuming that the turn angle is uniform throughout the fan modulation, the orientation of the magnetization in each monolayer can be uniquely determined such that the net magnetization perpendicular to the applied field is zero. Figure 11 interprets the evolution of (a)–(c) the fan modulation and (d)–(f) the helix modulation with the calculated values for the turn angle and opening angle. Only one period of the magnetic modulation is shown in Fig. 11. The numbers at the end of the arrows indicate the index of the Dy (0002) atomic layers. Although the period of the fan modulation remains at 11 monolayers from 130 to 153 K, the average turn angle and the average opening angle increase monotonically upon heating. This agrees with the decrease of the FM diffraction peak in Fig. 8(a). On the other hand, the turn angle of the helix modulation increases upon heating, resulting in the decrease of the period of the helix structure. Note that, in reality, the turn angles in the helix and fan modulations are unlikely to be uniform under the influence of the external field. The schematics in Fig. 11 only give an averaged picture on the evolution of the magnetic modulations.

Based on Figs. 8 and 11, the evolution of the magnetic phases upon heating in the field of 1 T can be described as:

(1) Between 119 and 130 K, the magnetizations in different Dy basal planes start to turn away from the field direction due to interplay between the RKKY interaction and the external field, and form a SRO fanlike structure. The transition is of the second order. The modulation of the fan structure is not well defined initially due to the inhomogeneity in the crystal.

(2) At $\sim$130 K, the lattice spacing between the (0002) planes is reduced abruptly (see Fig. 5), significantly modifying the magnetoelastic energy. The FM arrangement is no longer stable.

(3) As the temperature increases from 130 to 140 K, the LRO fan develops. The moments in the fan structure uniformly spread to a wider opening angle while the period of the fan remains at 11 monolayers.

(4) At ~140 K, a small fraction of the fan structure goes through a first-order transition to the helix structure. The turn angle is not modified during the transition, but the chirality of the magnetization is reversed for half of the monolayers.

(5) Heating from 140 to 153 K, more fan structure transforms into the helix structure. The turn angles for the helix and the remaining fan modulations grow monotonically but at different rates.

(6) At ~153 K, the transition to the helix is complete, when the period of the helix modulation is 10 monolayers.

(7) From 153 to 177 K, the period of the helix modulation further reduces to 9 monolayers.

(8) At ~177 K, the helix phase undergoes a second-order transition to the PM phase.

The intensity peaks of the diffuse scattering again confirm the critical temperatures of fan-helix and helix-PM transitions [Fig. 8(a)]. However, there is not enough evidence to verify the new phase at ~130 K suggested in Ref. [20].

E. Magnetic phases and the phase transitions of ^{163}Dy in the field of 1.5 T

With the field of 1.5 T applied along the a axis of the Dy crystal, the neutron diffraction scans were performed along the c axis from 114 to 190 K. The FM phase, a possible new phase, the fan phase, a possible helifan phase, and the PM phase were covered in this measurement according to the phase diagram in Ref. [20]. Again, (a) the integrated intensity and (b) the position of the magnetic diffraction peaks are plotted in Fig. 12. At 114 K, the FM phase dominates, while the fan phase emerges, as identified by the presence of magnetic satellites [see Fig. 13(a)]. Upon heating, the fan phase grows as evidenced by the increasing magnetic satellites [Fig. 13(b)]. The fan phase is most pronounced at ~155 K [Fig. 13(c)]. Above 177 K, the magnetic modulation turns into the PM phase, with only a small FM component induced by the external field [Fig. 13(d)]. However, the magnetic satellites do not immediately vanish at 177 K, suggesting some SRO fan structure still persists up to 190 K. The intensity of the FM peak decreases monotonically as the temperature increases from 114 to 177 K. The propagation wave vector of the fan modulation and its corresponding period in terms of the number of monolayers are plotted in Fig. 14. A closer look at the fan region in Figs. 12 and 14 suggests that the evolution of the fan phase can be divided into three stages:

(a) Between 114 and 142 K, the magnetic satellites are relatively weak and grow slowly compared to stage (b). The period of the magnetic modulation decreases from around 12 to 10 monolayers.

(b) From 142 to 160 K, the magnetic satellites grow at a higher rate compared to stage (a). The period of the magnetic modulation stays at around 10 monolayers.

(c) From 160 to 177 K, the magnetic satellites slowly fade. The period of the magnetic modulation decreases from around 10 to 8 monolayers.
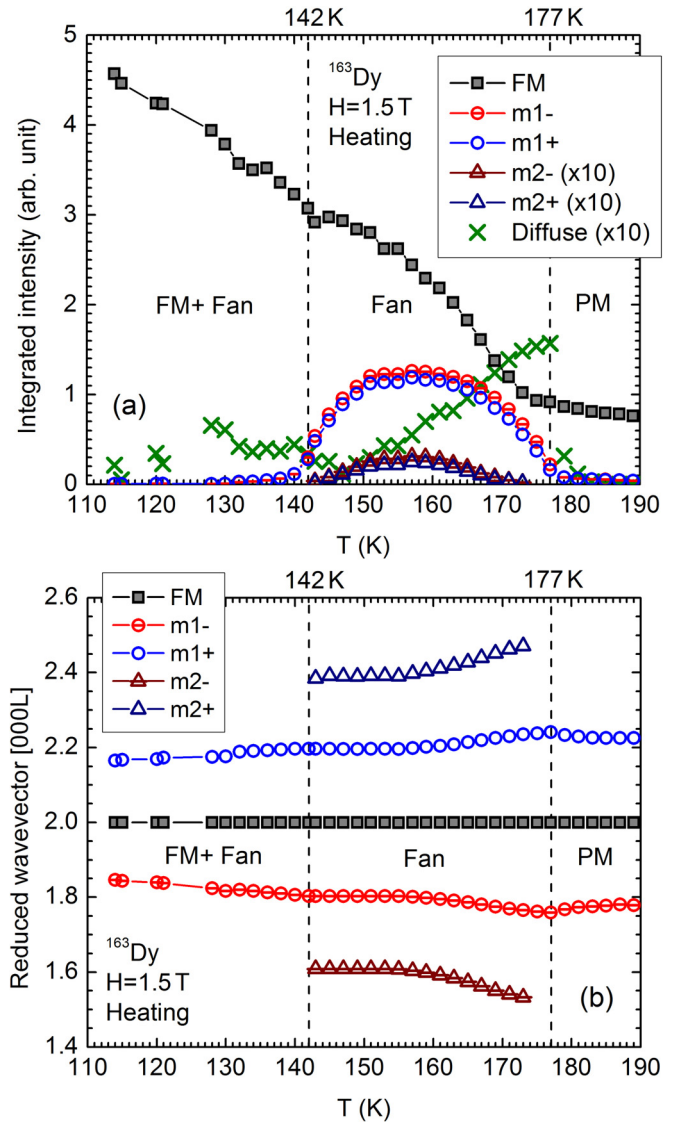

FIG. 12. (Color online) The temperature dependence of (a) the integrated intensity of the magnetic diffraction peaks and the diffuse scattering, and (b) the position of the peaks with 1.5 T field applied along the a axis of the Dy crystal. The intensities of the second-order magnetic satellites ($m2\pm$) and the diffuse scattering have been magnified by 10 times in order to show on the same scale as the FM diffraction peak and the first-order satellites ($m1\pm$). The dash lines indicate the phase boundaries between the coexisting FM and fan, fan, and PM phases.

The temperature ranges of the three stages match closely to the regions of the possible new phase, the fan phase, and the possible helifan phase indicated in Ref. [20].

Again, the average turn angle and the average opening angle of the fan structures were estimated based on the magnetization measured at 1.4 T reported in Ref. [20]. The schematics of the fan structure are shown in Fig. 15 for three different temperatures (128, 150, and 170 K), corresponding to the three stages of the fan phase. Based on Figs. 12 and 15, the following arguments can be made on the three stages of the fan phase upon heating in the field of 1.5 T:
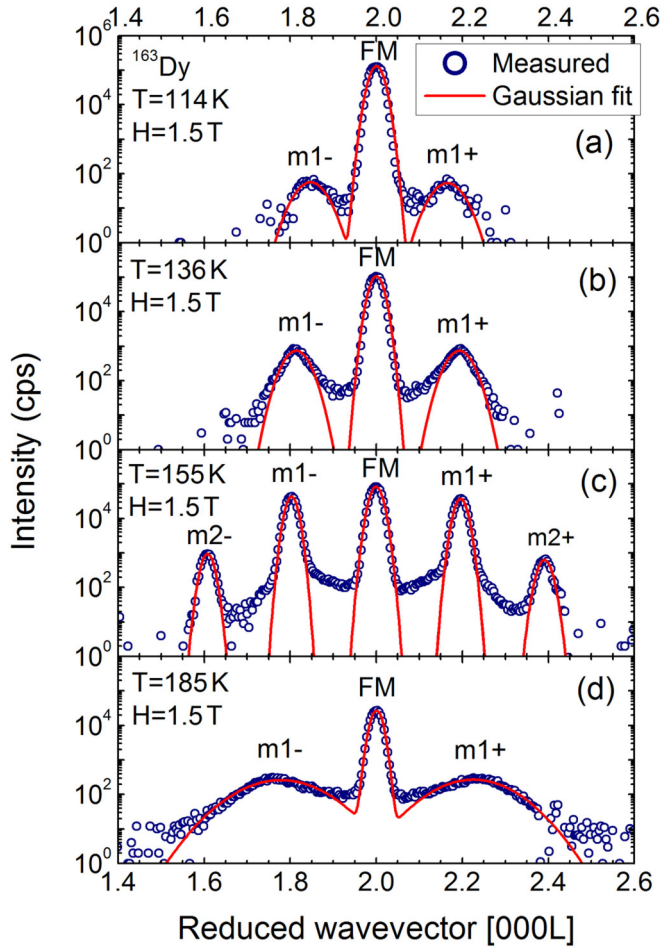
FIG. 13. (Color online) The diffraction patterns of pure magnetic origin (nuclear contribution subtracted) measured at (a) 114 K, (b) 136 K, (c) 155 K, and (d) 185 K when 1.5 T field is applied along the a axis of Dy. (a) and (b) are in the coexisting FM and fan phase; (c) is in the fan phase; (d) is in PM phase.
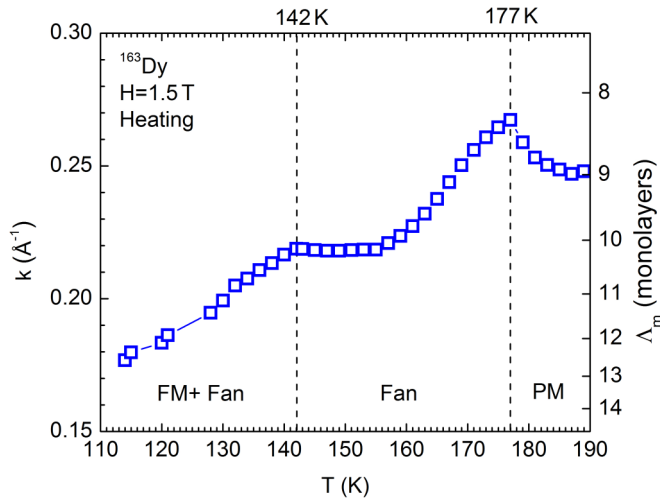

FIG. 14. (Color online) The temperature dependence of the propagation wave vector and the average period of the fan modulations in 1.5 T field applied along the a axis of the Dy crystal.
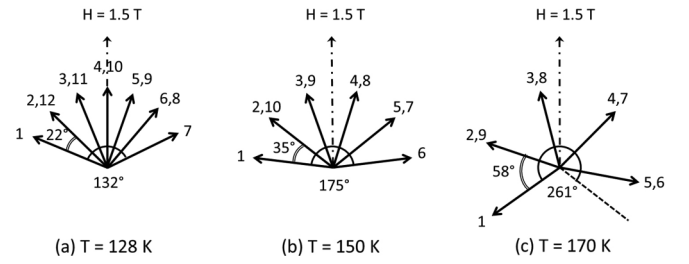

FIG. 15. The evolution of the spin arrangement for the fan modulation upon heating in the field of 1.5 T. Only one period of the magnetic modulation is shown. The average turn angle and opening angle are estimated based on the magnetization in Ref. [20]. The numbers at the end of the arrows indicate the indices of the Dy (0002) atomic layers.

(1) In stage (a) (114–142 K), the magnetizations in some of the monolayers start to turn away from the applied field direction and develop a fanlike modulation, while FM arrangement still persists in the other monolayers. Probably due to the effect of the crystal field anisotropy in the basal plane, the fan modulation in this region may involve spin-slip and is only SRO. The average period of the modulation decreases as the fan modulation becomes better defined upon heating.

(2) For stage (b) (142–160 K), a pronounced and LRO fan modulation develops rapidly, coupled with the c axis structural transition (see Fig. 5). The average turn angle of the fan grows monotonically but the period stays at 10 monolayers.

(3) In stage (c) (160–177 K), under the influence of thermal energy, the fan modulation becomes gradually disordered. Meanwhile, the average turn angle of the fan further increases, giving an average opening angle greater than 180° at 170 K. Between 170 and 177 K, the presence of a distorted helical modulation cannot be ruled out based on our scan along the c axis of the crystal. A scan along the b axis of the crystal may reveal the differences.

The intensity peaks of the diffuse scattering around 128, 142, and 177 K further confirm the phase boundaries between the aforementioned magnetic phases [Fig. 8(a)]. Both of the transitions at 142 and 177 K appear to be the second order. The absence of any outstanding helifan peak between the FM peak and the magnetic satellites rules out the possibility of well-defined helifan phase as seen in Ho [12,13]. This is consistent with the x-ray study performed on the lattice parameter of Dy in various fields [30] and mean-field calculations [18], which showed the free energy of the helifan phase is always greater than the free energy of the helix or fan phases.

F. The refined phase diagram

Based on the discussions above, we have refined the magnetic phase diagram of Dy around the region shown in Fig. 16. The possible new phase at ~140 K suggested in Ref. [20] is identified as an intermediate state between the FM and the LRO fan phase. It is mostly FM but contains SRO fan phase. The temperature region appears wider than that indicated in Ref. [20]. Some SRO fan arrangements also persist into the PM region. The boundary between the SRO and LRO fan is consistent with the onset of the c axis structural transition
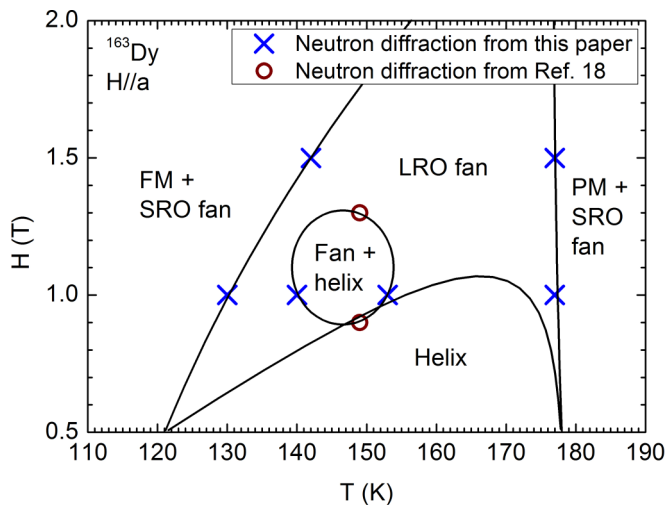
FIG. 16. (Color online) The refined magnetic phase diagram of Dy based on the neutron diffraction results, with the magnetic field applied along the *a* axis.

in 1 and 1.5 T. With the help from the data in Ref. [18], the small section of coexisting fan and helix has been mapped out.

IV. CONCLUSION

The neutron diffraction experiment was carried out by scanning along the *c* axis of a bulk ^{163}Dy crystal as a function of temperature with different fields (0, 1, and 1.5 T) applied in the *a* axis, covering the well-known FM, helical antiferromagnetic, and fan phases as well as several possible new phases suggested by the previous study. The *c* axis structural transition shifts to a higher temperature when a nonzero magnetic field is applied in the *a* axis. In a 1 T field, a second-order FM-fan transition, a first-order fan-helix transition, and a second-order helix-PM transition occur in sequence

upon heating. The fan phase is induced by the magnetic field; thus, it is suppressed in zero field as the first-order FM-helix transition takes place at the Curie temperature. In a 1.5 T field, the helix phase is suppressed, leading to a second-order fan-PM transition. The intermediate phase between FM and LRO fan consists of both FM and SRO fan arrangements. No trace of a well-defined helifan phase was observed throughout the temperatures. The phase boundaries are determined by the temperature dependence of the magnetic diffraction peaks as well as the diffuse scattering. Taking into account of the newly determined magnetic origin of the field induced phases, the magnetic phase diagram of Dy has been refined to include the SRO/LRO fan phase, as well as the coexisting helix/fan region. The modulation period of both the fan and helix phases decreases upon heating. Estimated from the period of the magnetic modulation and the average magnetization, a quantitative picture is given on the evolution of the spin arrangement in the fan and helix phases. These behaviors can be understood by considering the competition between the RKKY exchange interaction, the crystal field anisotropy, the magnetostrictive interactions, and the Zeeman interaction.

[1] J. Jensen and A. R. Mackintosh, *Rare Earth Magnetism* (Clarendon, Oxford, 1991).

[2] M. K. Wilkinson, W. C. Koehler, E. O. Wollan, and J. W. Cable, J. Appl. Phys. **32**, S48 (1961).

[3] D. Gibbs, J. Bohr, J. D. Axe, D. E. Moncton, and K. L. D'Amico, Phys. Rev. B **34**, 8182(R) (1986).

[4] H. Miwa and K. Yosida, Progr. Theor. Phys. **26**, 693 (1961).

[5] K. Yosida and H. Miwa, J. Appl. Phys. **32**, S8 (1961).

[6] R. M. Nicklow, J. Appl. Phys. **42**, 1672 (1971).

[7] R. J. Elliott, Phys. Rev. **124**, 346 (1961).

[8] W. E. Evenson and S. H. Liu, Phys. Rev. **178**, 783 (1969).

[9] W. C. Koehler, Acta Crystallogr. **14**, 535 (1961).

[10] W. C. Koehler, J. Appl. Phys. **36**, 1078 (1965).

[11] J. W. Cable, E. O. Wollan, W. C. Koehler, and M. K. Wilkinson, J. Appl. Phys. **32**, S49 (1961).

[12] J. Jensen and A. R. Mackintosh, Phys. Rev. Lett. **64**, 2699 (1990).

[13] T. Kosugi, S. Kawano, N. Achiwa, A. Onodera, Y. Nakai, and N. Yamamoto, Physica **334**, 365 (2003).

[14] D. Gibbs, D. E. Moncton, K. L. D'Amico, J. Bohr, and B. H. Grier, Phys. Rev. Lett. **55**, 234 (1985).

[15] R. A. Cowley and S. Bates, J. Phys. C: Solid State Phys. **21**, 4113 (1988).

[16] F. Galeener and J. Blackman, *Disorder in Condensed Matter Physics* (Oxford Science Publications, Oxford, 1991).

[17] R. Herz and H. Kronmüller, J. Magn. Magn. Mater. **9**, 273 (1978).

[18] N. Wakabayashi, J. W. Cable, and J. L. Robertson, Physica B **241–243**, 517 (1997).

[19] M. Akhavan, H. A. Blackstead, and P. L. Donoho, Phys. Rev. B **8**, 4258 (1973).

[20] A. S. Chernyshov, A. O. Tsokol, A. M. Tishin, K. A. Gschneidner, and V. K. Pecharsky, Phys. Rev. B **71**, 184410 (2005).

[21] F. J. Darnell, Phys. Rev. **130**, 1825 (1963).

[22] T. Chatterji, *Neutron Scattering from Magnetic Materials* (Elsevier, Amsterdam, 2006).

[23] O. W. B. Schult, M. E. Bunker, D. W. Hafemeister, E. B. Shera, E. T. Jurney, J. W. Starner, A. Bäcklin, B. Fogelberg, U. Gruber, B. P. K. Maier, H. R. Koch, W. N. Shelton, M. Minor, and R. K. Sheline, Phys. Rev. **154**, 1146 (1967).

[24] Miller-Bravais indices are used in this paper since the Dy crystal is hcp structure. F. C. Frank, Acta Crystallogr. **18**, 862 (1965).

[25] J. J. Rhyne, Ph.D. thesis, Iowa State University, 1965.

[26] J. J. Rhyne and T. R. McGuire, IEEE Trans. Magn. **8**, 105 (1972).

[27] T. A. Kaplan, Phys. Rev. **124**, 329 (1961).

[28] U. Enz, J. Appl. Phys. **32**, S22 (2009).

[29] T. Nagamiya, J. Appl. Phys. **33**, 1029 (2004).

[30] Y. Kida, K. Tajima, Y. Shinoda, K. Hayashi, and H. Ohsumi, J. Phys. Soc. Jpn. **68**, 650 (1999).